

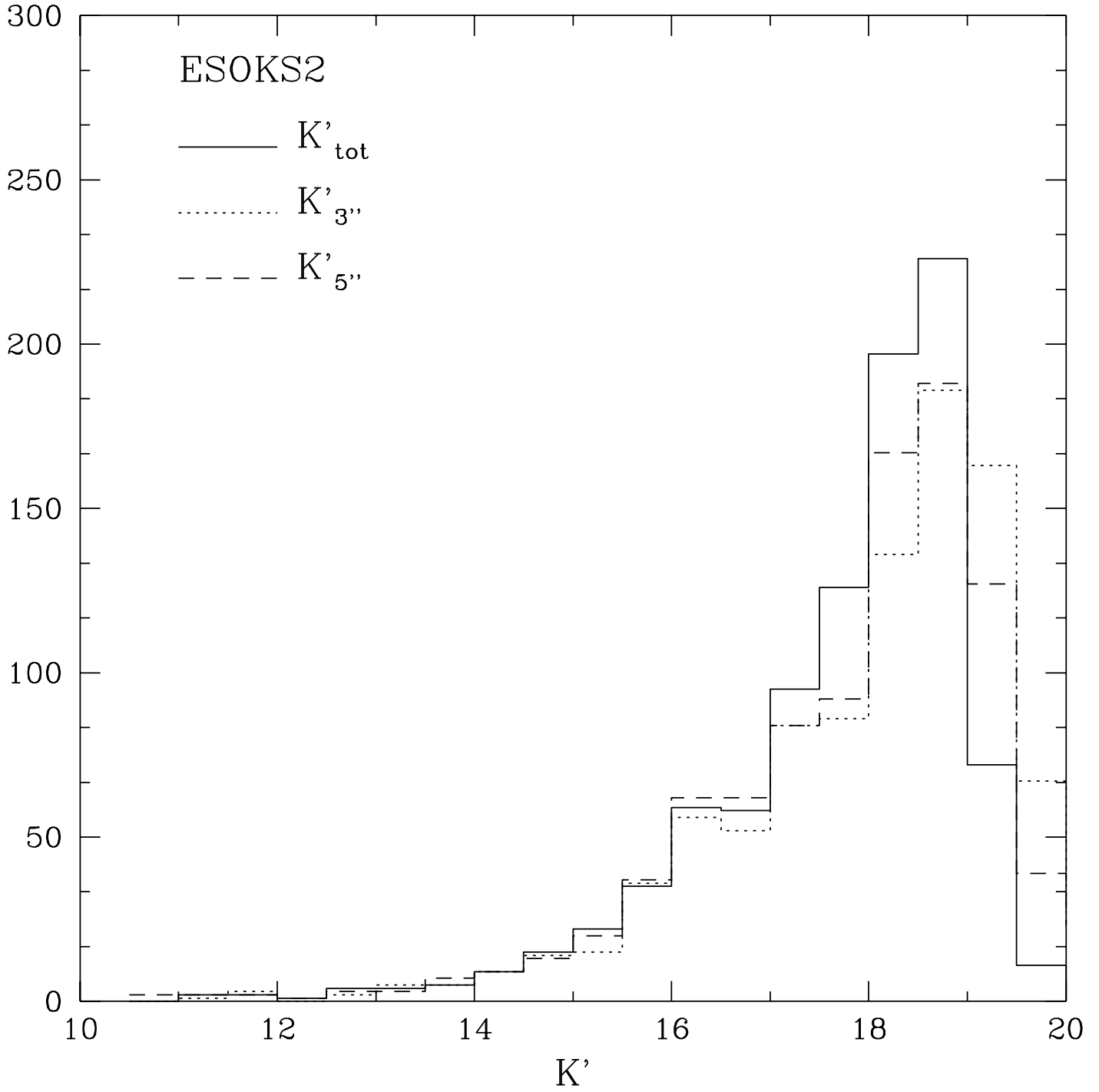
ESOKS2

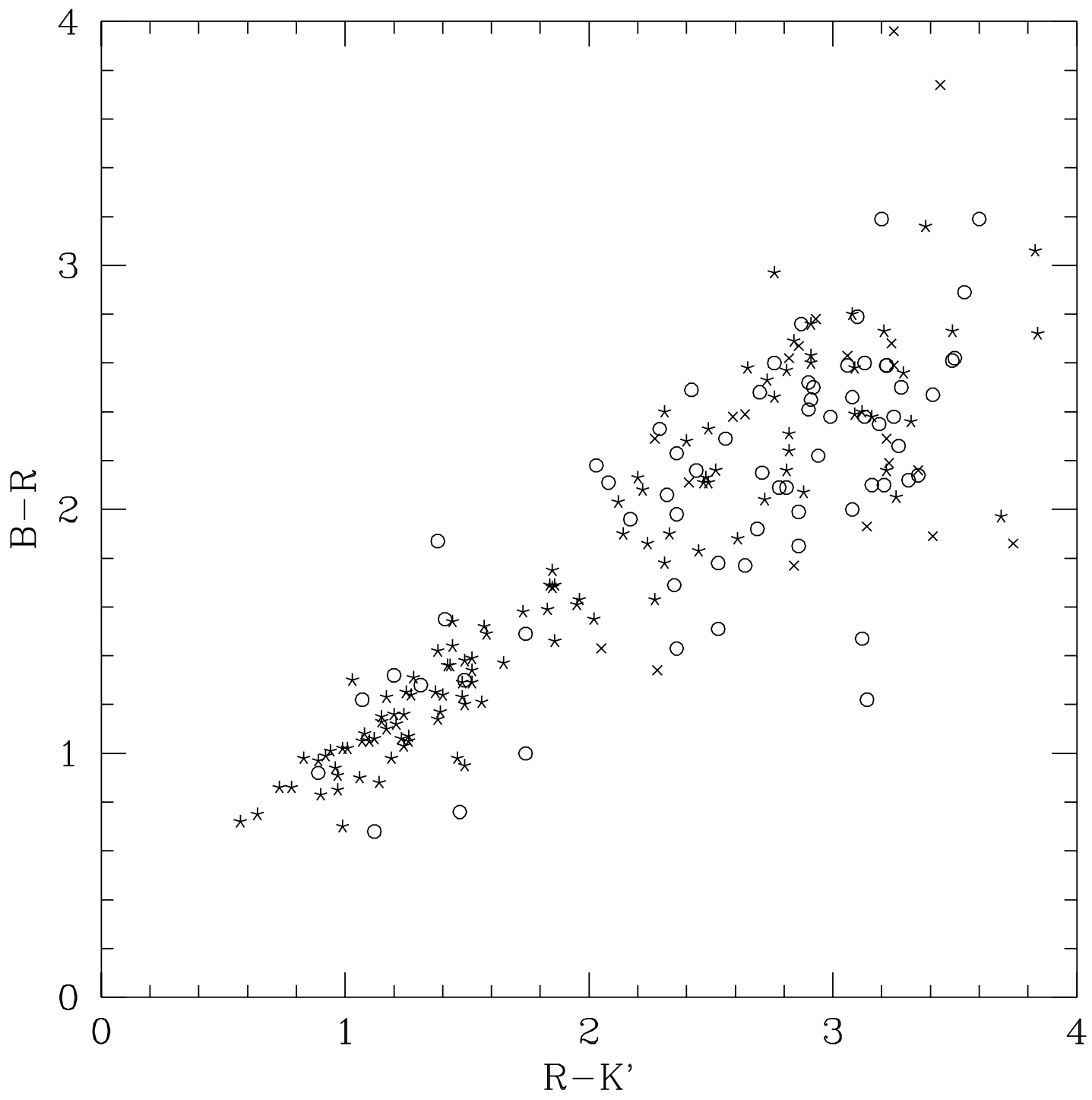
— K'_{tot}

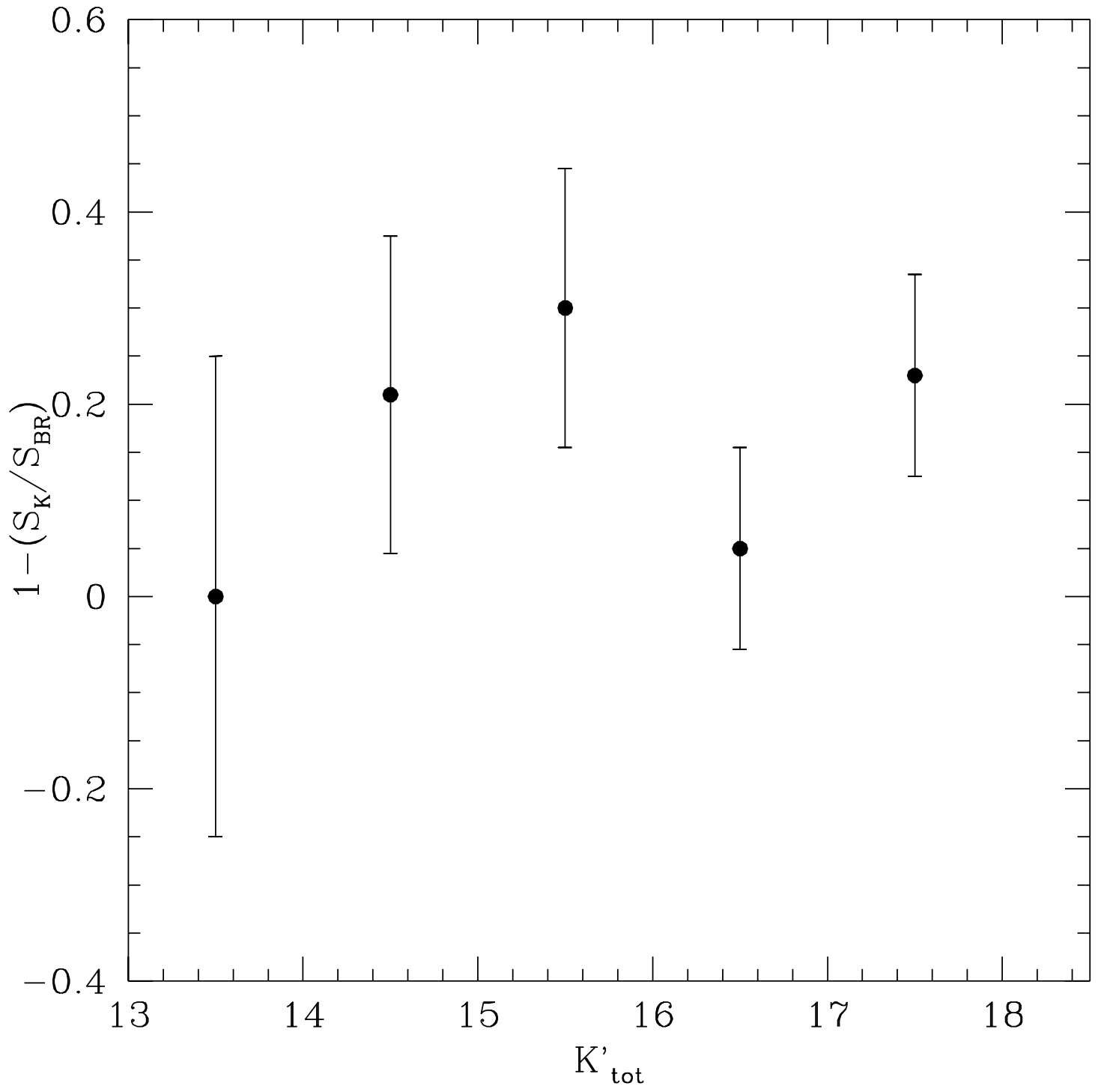
⋯ $K'_{3''}$

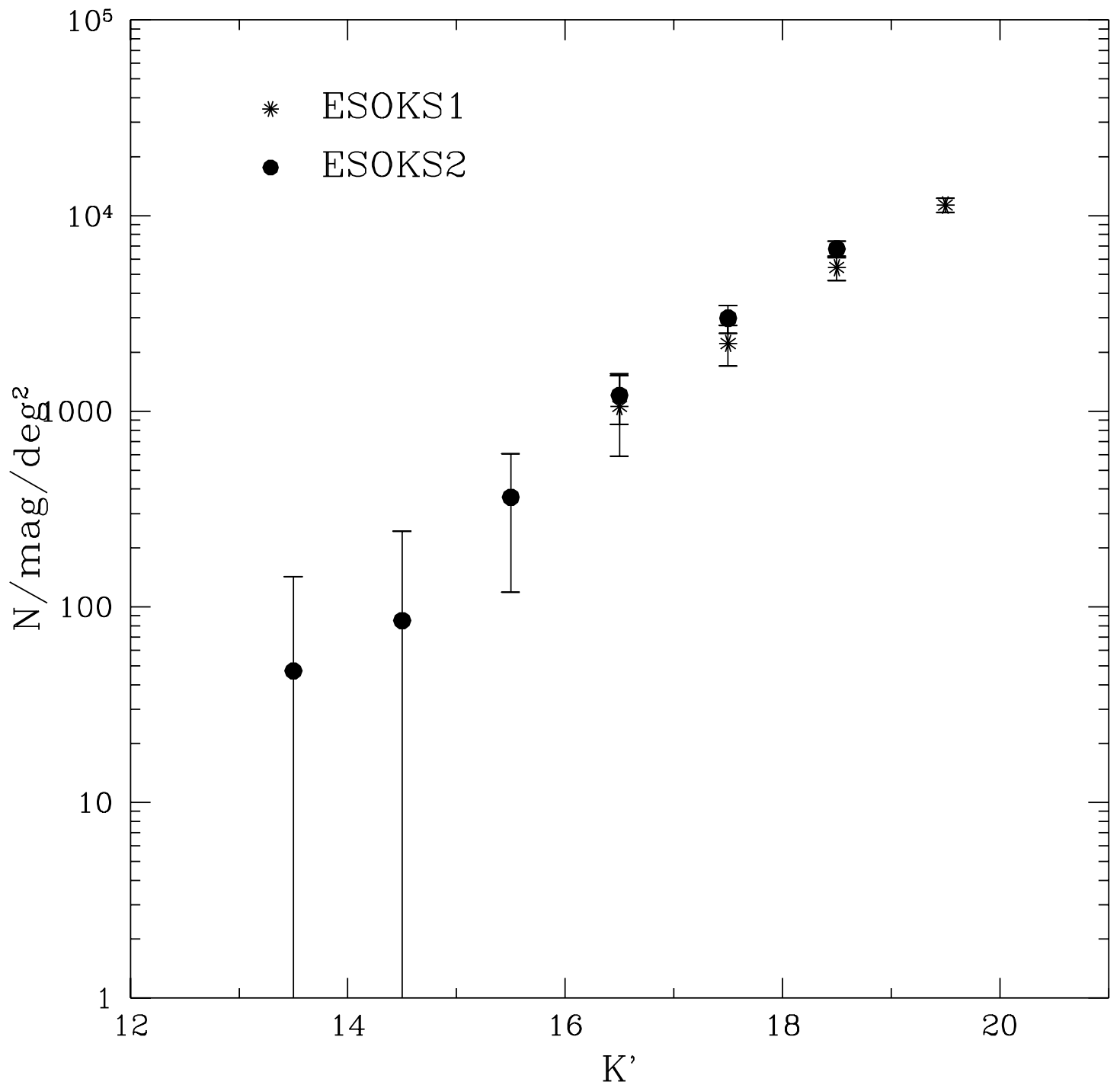
- - $K'_{5''}$

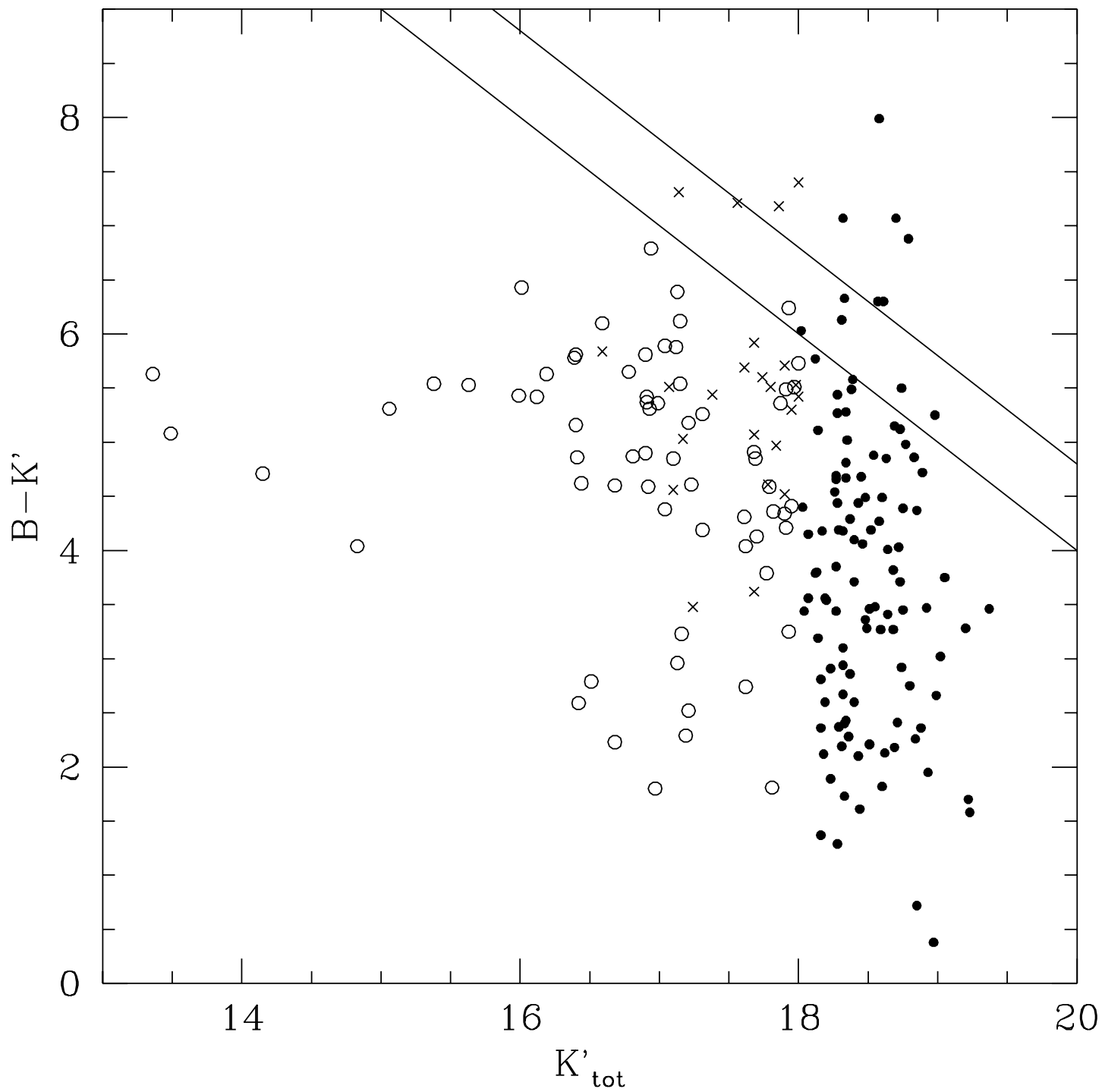
Number of Sources

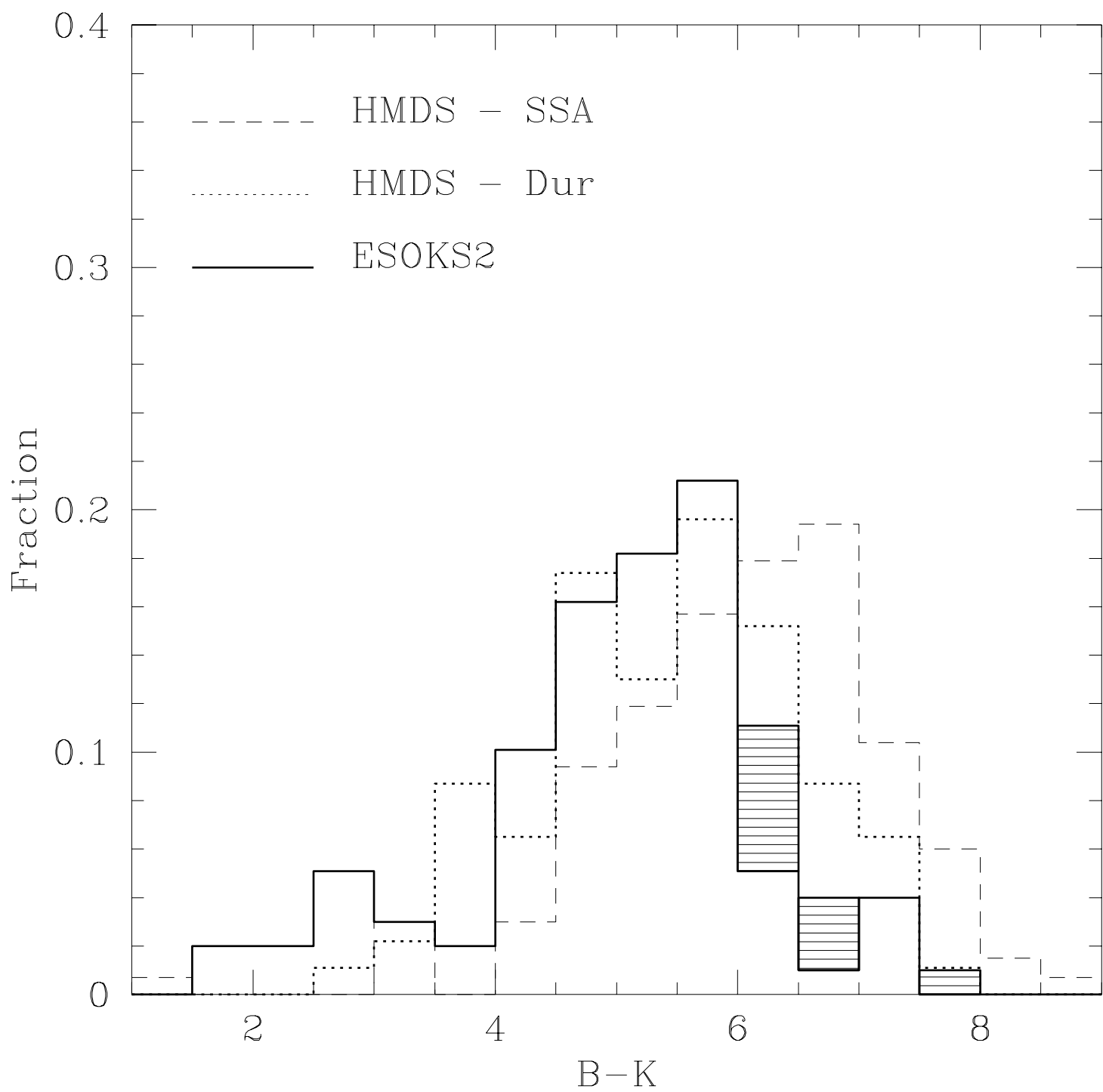


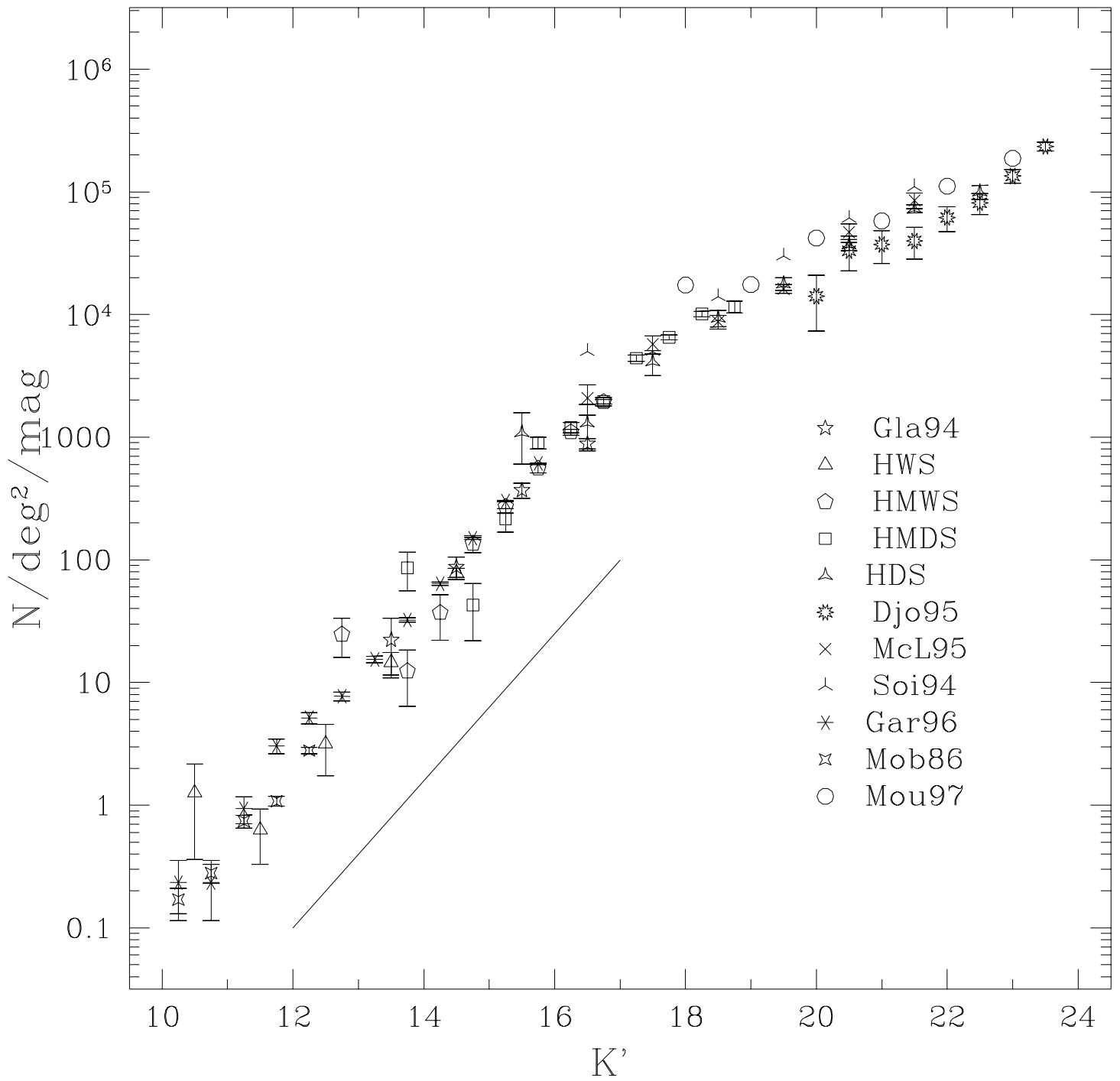


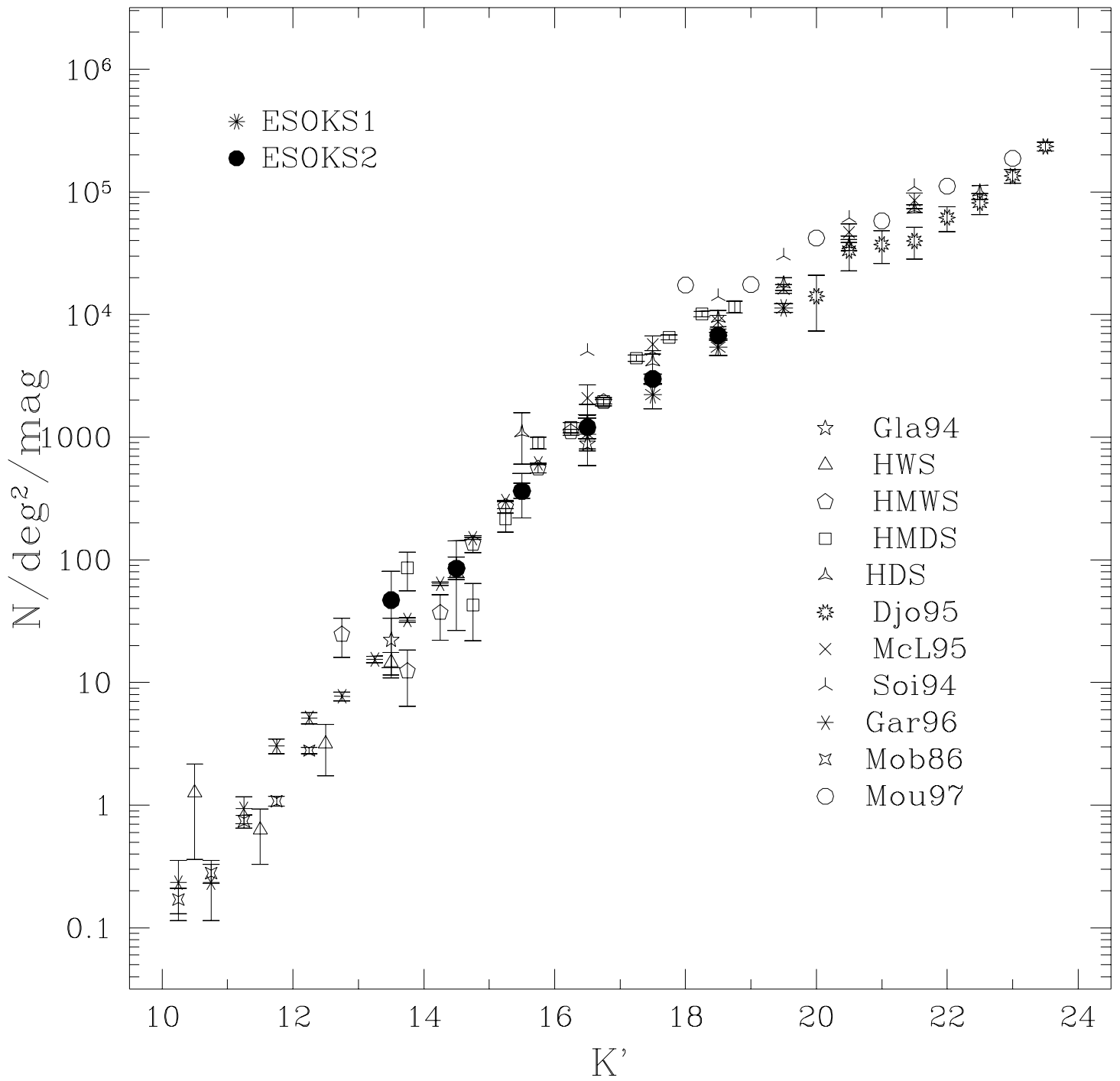








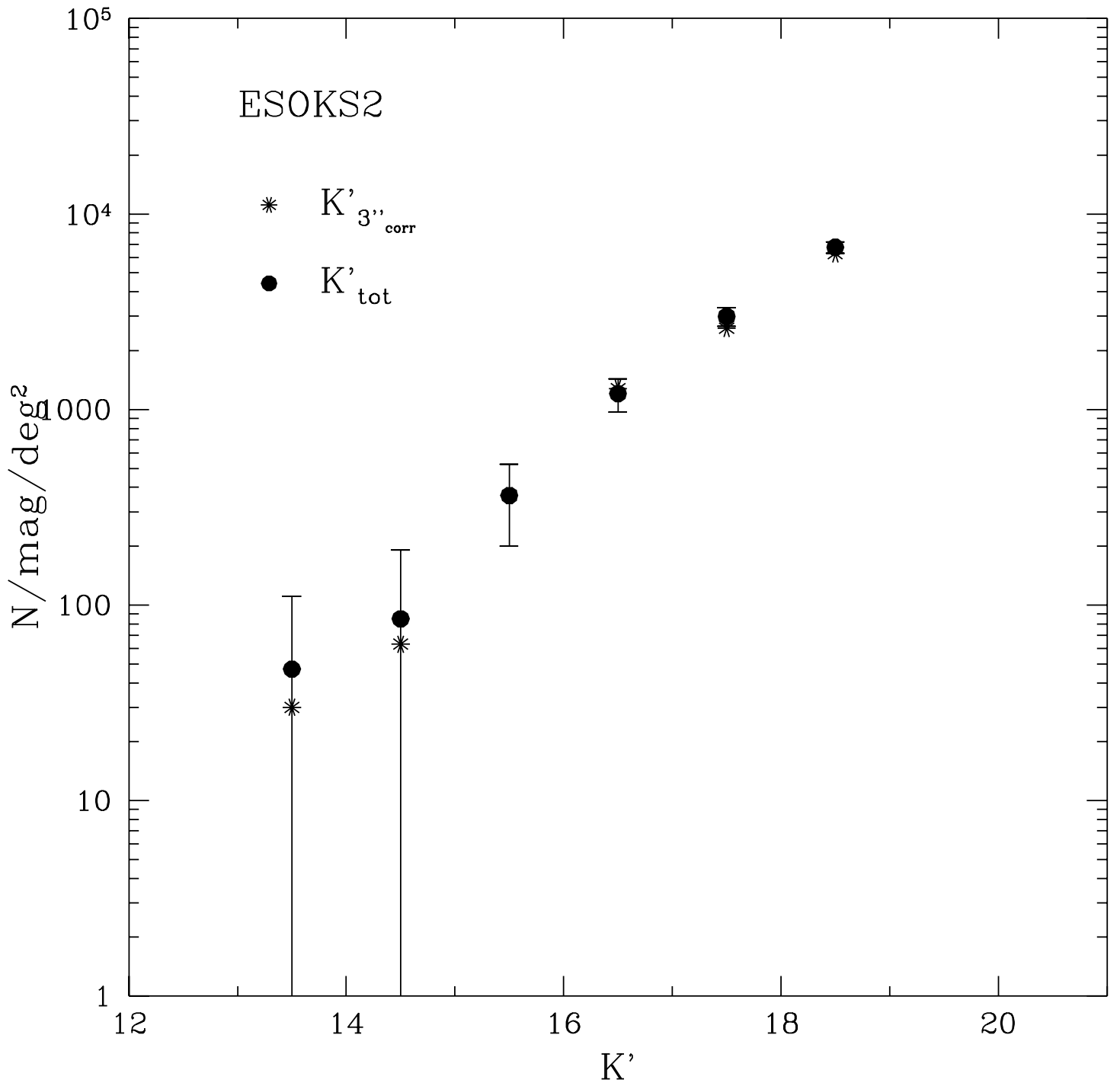




ESOKS2

* $K'_{3''_{\text{corr}}}$

● K'_{tot}



The ESO K' -Band Galaxy Survey Galaxy Counts¹

P. Saracco¹, A. Iovino², B. Garilli¹, D. Maccagni¹ and G. Chincarini^{2,3}

¹ Istituto di Fisica Cosmica del CNR, Via Bassini 15, 20133 Milano, Italy

² Osservatorio Astronomico di Brera, Via Brera 28, 20121 Milano, Italy

³ Dipartimento di Fisica, Università di Milano, Via Celoria 16, 20133 Milano, Italy

ABSTRACT

We present K' -band galaxy counts in the magnitude range $13 < K' < 20$, obtained from two independent surveys near the South Galactic Pole, covering an area of ~ 40 arcmin² and ~ 170 arcmin², including ~ 200 and ~ 1000 objects respectively up to a magnitude limit $K' \sim 20.0$ and $K' \sim 19.0$. At magnitudes $K > 18.5$ we surveyed an area more than 7 times wider that covered by previous K -band surveys. Our counts are quite in good agreement with those in the literature at magnitudes brighter than $K \sim 17$, while are systematically lower at fainter magnitudes. We confirm a change in the slope of the $d\log N/dm$ relation at $K' \sim 17$ from 0.57 to 0.35, but do not find the bump shown by other K -band surveys in the magnitude range $16 < K < 20$. Furthermore 10% of the galaxies brighter than $K' \sim 18$ have $B - K' < 3$. We suggest that these blue objects represent a population of sub- L^* nearby evolving galaxies.

Subject headings: cosmology: observations – galaxies: general – infrared: galaxies

¹Accepted for publication in The Astronomical Journal

1. Introduction

Present day ground based instrumentation allows to count galaxies fainter than $B=27$ (Tyson 1988; Metcalfe et al. 1995) and the resulting $d\log N/dm$ relation shows an excess of galaxies with respect to the predictions of a no-evolution model. Several authors have tried to explain such an excess suggesting some mild luminosity evolution, or more complex mechanisms (White 1989; Broadhurst et al. 1992; Cowie et al. 1991).

Recent results from HST observations cast new light on this problem. Driver et al. (1995), Glazebrook et al. (1995) and Abraham et al. (1996) show that while elliptical and early-type spiral number counts are in good agreement with the predictions of no-evolution models, late-type/irregular galaxies show an excess with respect to such predictions. Driver et al. (1996) also find that most of the faint blue galaxy excess at $B \sim 23.5$ is due to a population of evolving dwarf galaxies at $0.2 < z < 0.5$, even if it is unclear which kind of evolution they should undergo. In general, galaxy counts in the visible bands suggest that late Hubble types undergo some evolution at redshifts $z \leq 0.5$. It should be noted, however, that optically selected samples tend to favor star forming galaxies (i.e. evolving galaxies) and this is even more true in the B band.

Near-infrared (IR) selection may provide significant advantages over optical selection in the study of galaxy evolution: k-corrections are small and nearly independent on galaxy type (Cowie et al. 1994); the sample is less biased towards star-forming galaxies; the comparison models are simpler. Already from the first survey (Cowie et al. 1990), it was immediately realized that K-band counts do not require galaxy evolution. Such a discrepancy between B-band and K-band counts has been confirmed by all the subsequent K-band surveys, which have extended the counts down to $K \sim 22.5$ (Gardner et al. 1993; Cowie et al. 1994; Soifer et al. 1994; McLeod et al. 1995) and to $K \sim 24$ (Djorgovski et al. 1995). The signatures of evolutionary changes are however present also in the IR counts: K-band counts flatten at magnitudes $K \sim 17$ (Gardner et al. 1993) and a blueing of the galaxies occurs at fainter magnitudes (Gardner et al. 1993; Cowie et al. 1995). These two observational evidences imply that field galaxies undergo substantial changes at $K \sim 17-18$, which is the expected magnitude of an L^* galaxy at $z \sim 0.3$. Colless et al. (1993; 1994) and Griffiths et al. (1994a,b) have shown that, at these redshifts, there is an increase of starburst activity, mainly associated with tidal and merging phenomena, while Driver et al. (1996) show that a large fraction of dwarfs present at $z \sim 0.5$ has subsequently faded to obscurity.

Thus, our understanding of galaxy evolution would greatly benefit from a *large, IR-selected* sample of galaxies in the magnitude range $15 < K < 20$. Such a sample is still missing. The deep IR surveys go fainter than $K \sim 18$ (Cowie et al. 1990; Cowie et al.

1994; Soifer et al. 1994; McLeod et al. 1995; Djorgovski et al. 1995; Moustakas et al. 1997) but cover small areas (from ~ 1 to ~ 20 square arcminutes), thus giving small numbers of galaxies at magnitudes $K < 17-18$. On the other hand, the limiting magnitudes of shallower surveys (covering larger areas) are either brighter than $K = 16$ (Gardner et al. 1996; Huang et al. 1997) or fall in the range $17 < K < 18$ (Glazebrook et al. 1994; Gardner 1995a), which implies a possible incompleteness at these magnitudes.

At the end of 1993 we started a project aimed at selecting an IR galaxy sample deep and large enough to study galaxy evolution. The project consists of two surveys: the ESOKS1 (ESO K' -band Survey 1) limited to $K' = 20$ over ~ 40 arcmin² of sky and mainly designed to define faint galaxy counts and to study faint objects, and the ESOKS2 limited to $K' \sim 19$ over a region of ~ 170 arcmin², making up the bulk of our sample for $K' \leq 19$.

In this paper we describe the two surveys and the analysis of the ensuing galaxy counts.

2. The Surveys

2.1. Field Selection

The fields observed in the two independent surveys were selected in two slightly different ways and cover unconnected areas.

ESOKS1: We selected 12 fields according to the following criteria:

1. each field had to be at high galactic latitude ($b < -45^\circ$), in order to minimize star contamination and galactic extinction;
2. all fields had to include two medium brightness stars ($17.5 \leq b_j \leq 19$), in order to optimize the stacking of the different IR frames;
3. the fields had to be free from clearly visible objects in the ESO–SRC sky survey plates (apart from the two stars of point 2).

This last requirement was intended to avoid having a significant part of the field covered by bright galaxies, being the ESOKS1 aimed at defining galaxy counts at magnitudes fainter than $K' = 16$ (down to $K' \sim 20$) and to construct a faint object catalog. Obviously, this criterion introduces a bias against $b_j < 20.5$ objects. From the B-band galaxy counts (e.g. Tyson 1988; Maddox et al. 1990; Jones et al. 1991; Metcalfe et al. 1991; Bertin &

Dennefeld 1997) we would expect to find 7-9 such galaxies in the ~ 40 arcmin² of the survey. According to the $B - K'$ color distribution of the B -selected galaxy sample of Bershadsky et al. (1994), only 1 of these galaxies should be in the range $16 < K' < 17$ and only 0.2 galaxies in the range $17 < K' < 18$. Since the expected number of galaxies fainter than $K' \sim 16$ is $\gg 1$ in the ESOKS1 area, this bias is negligible.

ESOKS2: The purpose of this second survey was to explore a larger area, reaching magnitude limits brighter than ESOKS1 (down to $K' \sim 19$). We randomly selected 51 fields according to the first two selection criteria and dropped the last criterion in order to construct a sample unbiased with respect to bright and blue objects. However, because of observing time scheduling, it was not possible to select all the fields at high galactic latitude. In particular 13 fields are at $-45^\circ < b < -20^\circ$, while the remaining 38 fields are at high galactic latitude ($b < -45^\circ$).

In Table 1 and 2 we give the right ascension, declination and the galactic latitude of the center of each field, and the integration time (t_{exp}) for each of the ESOKS1 and ESOKS2 fields respectively.

2.2. Observations

Observations were made at the ESO 2.2m telescope equipped with the IRAC2B infrared camera (Morwood et al. 1992). This camera is based on a NICMOS3 array (Hodapp et al. 1992) of 256×256 HgCdTe diodes. With objective C, the pixel size is 0.5 arcsec, thus providing a field of view of 2.1×2.1 arcmin and a reasonable sampling of the object profiles under average seeing conditions.

The data were obtained using the K' filter ($\bar{\lambda} = 2.15\mu\text{m}$ and $\Delta\lambda \sim 0.32$). Tests performed at the ESO 2.2 m telescope show that through the K' filter the sky+telescope background is 35% lower than through the standard K filter, yielding a 20% reduction in sky noise (Lidman et al. 1995).

The 12 ESOKS1 fields were observed on October 5 through 7, 1993. The seeing was in the range 1-1.5 arcsec. One field was observed for $t_{exp} = 36$ min, 7 fields for $t_{exp} = 54$ min, 2 fields for $t_{exp} = 72$ min and the remaining 2 fields for $t_{exp} = 162$ min. The 51 fields of the ESOKS2 were observed during a run of 5 nights starting on August 25, 1995. The seeing was in the range 0.9-1.3 arcsec. The exposure time was 36 minutes for 50 out of the 51 observed fields, and 18 minutes for the remaining one.

Due to the brightness of the background ($\sim 12.6 K'$ mag arcsec $^{-2}$ from a combination of sky, telescope and instrument, Morwood et al. 1992), extremely accurate flat-fielding is required (about 1 part in 10^4 in each pixel) to reach a magnitude limit of $K' \sim 20$. In order to achieve this result the "shift and stare" observational technique (Tyson 1989) was adopted. We obtained 9 frames around the center of each field by moving the telescope by 10 arcseconds each time in a well defined grid pattern. In order to avoid pixel saturation effects, each frame is the average of 12 exposures of 10 s each, and the central 1.8×1.8 arcmin of each image, obtained from the stacking of the 9 mosaic frames, has an exposure time of 18 min. Longer exposure times are obtained by repeating the pattern. This technique allows to have sky limited exposures while keeping the overheads to a reasonable small fraction of the total observing time.

14 fields at $b > -60^\circ$ out of the 51 fields of the ESOKS2 have also been observed in the B and R bands (they are marked with * symbol in Table 2). These observations were obtained at the ESO 0.9 m Dutch telescope in August 1995, with exposure times of 60 minutes in the B -band and 30 minutes in the R -band. The pixel size is 0.44 arcsec and the seeing, throughout the observations, was in the range 1.3-1.8 arcsecs. Here we present the colors of the galaxies in these fields in the framework of the K galaxy counts.

2.2.1. Photometric Accuracy

Absolute photometry was obtained by observing standard stars taken from the lists of Elias et al. (1982) and Legget & Hawkins (1988) with magnitudes in the range $8 < K < 11.5$. During each night we observed from six to eight standard stars evenly spaced in time. Each individual frame was the average of 12 exposures of 2 seconds each. We derived K' magnitudes from the relation

$$K' - K = (0.20 \pm 0.04)(H - K) \tag{1}$$

(Wainscoat & Cowie 1991). The typical scatter in the zero-point is 0.05 mag for the ESOKS1, and on the order of 0.03 mag for the ESOKS2.

3. Data Reduction

Data reduction and analysis was based on the IRAF data reduction package. After correction for the dark current, for each frame we constructed its own median sky-flat, using an adequate number of adjacent frames. Since the sky color changes over time scales on the order of ~ 15 min (e.g. Glazebrook et al. 1994), no more than 7-8 time-adjacent frames

can be used to construct the flat-field of each frame. On the other hand, a good sampling of the pixel response is only obtained from a sufficiently high number of frames. We found that the best compromise is to combine 6-7 time-adjacent frames to obtain the sky flat of each image, taking care to remove objects and cosmic rays using a median sigma-clipping rejection algorithm. Each frame was then flat-field corrected and a constant sky value subtracted. The resulting sky-subtracted flat-fielded frames were registered and combined with median weights. In order to optimize the co-adding, each frame was re-sampled with smaller pixel size taking care to preserve the flux. In the resulting final frames, both the pixel-to-pixel variations and the large scale spatial variations are on the order of 10^{-4} counts per pixel.

4. Detection, Completeness and Photometry: Simulations

Source detection was performed using FOCAS (Jarvis & Tyson 1981; Valdes 1982). As the detection algorithm is based on two main parameters, detection threshold and minimum number of connected pixels satisfying the threshold criterion and defining the source, detectability primarily depends on the S/N ratio of the pixels defining an object and on their being contiguous. Optimization of the two algorithm parameters allows to push the detection to the faintest limits, while keeping low the number of spurious detections. Incompleteness increases as low surface brightness objects fall below the detection threshold. In order to evaluate the corrections for incompleteness and the contamination due to spurious detections, we carried out a set of simulations.

We constructed ten background frames (noise frames) by combining the appropriate number of different flat-fielded 2 min frames for each exposure time. Cosmic rays and objects from the different frames were removed by taking the median of the pixel intensity in each frame.

Simulated galaxies were then added to each background frame. We divided the magnitude range $18.0 < K' < 20.0$ into four 0.5 mag wide bins, and magnitudes were randomly assigned to each galaxy within each bin so that a log(number)-magnitude relation with slope 0.6 was globally reproduced. For each bin, we simulated 300 galaxies, assuming a morphological mix of 35% early type galaxies (E+S0) and 65% late type galaxies (Guiderdoni 1991). Early type galaxies were assumed to have a de Vaucouleurs profile and spirals a pure exponential one; ellipticities and position angles were randomly assigned to each galaxy and the effect of clustering was not included. The apparent size of each galaxy was rescaled following the diameter-distance relation, assuming that all galaxies have luminosity L^* . Each galaxy was convolved with a Moffat function with a FWHM of

1.25 arcsec, which is a fairly good approximation to our seeing profile. A galaxy having an absolute magnitude on the order of L^* and an apparent magnitude of $K' \sim 18.5$, has an apparent effective radius $\theta < 0.5$ arcsec, irrespective of its intrinsic profile. Therefore, at magnitudes fainter than $K' \sim 18.5$ most of the objects are pointlike in our frames, and both detection and completeness do not depend on galaxy profiles and/or morphological mixture. Then, we added each set of 300 galaxies to the 10 noise frames (30 galaxies per frame per magnitude bin). This procedure was repeated for the different exposure times.

To increase the signal-to-noise ratio, and therefore the detectability of the sources, we convolved the simulated images with a pass-band filter (boxcar) having a running window slightly greater than the seeing disk (see Bernstein et al. 1995; Banchet et al. 1997; Mamon 1995). We applied the FOCAS detection algorithm to the convolved images trying different values of detection threshold and area: the best results (i.e. the lowest number of spurious detections and a high completeness) were obtained with a detection threshold of 3σ per pixel and a minimum detection area $\sim 50\%$ greater than the seeing disk. In Table 3 the derived completeness correction factor c is shown for each magnitude bin as a function of the exposure time.

Three different types of magnitudes can be computed with FOCAS: isophotal (K'_{iso}), fixed aperture (K'_{apr}) and total magnitude (K'_{tot}). The isophotal magnitude is calculated within the detection isophote, while the total magnitude is derived by growing the object several pixels in all directions around the original detection isophote and measuring the flux above the sky inside this expanded region. We chose apertures of 3 and 5 arcsec in diameter, i.e. at least twice the largest FWHM of the seeing disk in our images. To decide which of these different quantities best approximates the "real" magnitude of the galaxies, we have compared them with the magnitudes m_{true} of the simulated galaxies. Even if the best agreement is obtained between K'_{tot} and m_{true} , FOCAS total magnitudes tend to systematically underestimate the flux of the sources fainter than $K' \sim 17.5$ (ESOKS2) and $K' \sim 18.5$ (ESOKS1). By comparing the estimated and the simulated flux we computed the correction to be applied to K'_{tot} : the applied corrections are 0.06, 0.15, 0.25 and 0.35 mag for sources in the magnitude range $17.5 < K' < 18$, $18 < K' < 18.5$, $18.5 < K' < 19$ and $K' > 19$ respectively. After this correction the scatter of $\Delta m = K'_{tot} - m_{true}$ is $\sigma_{\Delta m} \sim 0.2$ for galaxies with $19.0 < K'_{tot} < 20$ in the case of $t_{exp} \geq 54$ min (ESOKS1). The same scatter is present for sources in the range $18 < K'_{tot} < 19$ for $t_{exp} \leq 36$ min (ESOKS2). The scatter decreases rapidly going to brighter magnitudes and it is ~ 0.1 mag at $K' < 19$ ($t_{exp} \geq 54$ min) and $K' < 18$ ($t_{exp} = 36$ min). Therefore we consider 0.2 mag as our typical uncertainty on the faintest magnitudes.

5. Image Analysis

5.1. Source Detection and Photometry

The detection procedure described above was applied to the real frames. Over the ~ 40 arcmin² of the ESOKS1, 198 objects with magnitudes $K'_{tot} \leq 20$ were detected, while 998 sources brighter than $K'_{tot} = 19.5$ were detected over the ~ 170 arcmin² of the ESOKS2. In Fig. 1 and Fig. 2 the K'_{tot} magnitude distributions for the two samples are shown. In Fig. 2, also the $K'_{3''}$ and $K'_{5''}$ magnitude distributions are plotted. The distributions of the three different magnitude estimates are in good agreement down to $K' = 18$. At fainter magnitudes the three distributions are slightly different since both the 3 and 5 arcsec apertures tend to underestimate the source flux, even if the differences are within 1σ . Thus we do not expect a significant dependence of the number counts on the particular method chosen to estimate the magnitude. From now onwards we will use K'_{tot} magnitudes (corrected as specified in Section 4) unless explicitly stated.

In the 14 fields observed also in the B and R bands, there are 398 K' -detected objects: 312 of these objects are also detected in both B and R .

5.2. Star-Galaxy Separation

There are several methods to separate stars from extended objects, including the purely statistical one, based solely on star counts models.

Gardner (1995b) and McLeod et al. (1995) base their classification on source colors: given 3 filters, B , K and X , where X is a third red band, in the color–color diagram $B - X$ vs $X - K$ main sequence stars define a specific locus, while normal galaxies are expected to lie in the lower part of the diagram. On the contrary, Metcalfe et al. (1991) base their classification on the isophotal area: at a given magnitude, stars should have a smaller isophotal area than galaxies. Having observed the 14 fields at low galactic latitude also in the optical bands with a much higher S/N, we checked the applicability of both these methods to our data. We ran the FOCAS classifier (which takes into account the first moment of the radial distribution of the light of the source) on both the B and R images and considered as classified those sources for which the classification coincided. The reliability of this classification was checked on the brighter sources by visual inspection. We have coincident classifications for 85% of the sources down to $K' = 18$ (214 sources). In Fig. 3 we present the $B - R$ vs $R - K'$ color–color plot for the classified objects (stars represent stars and open circles galaxies), and for the unclassified objects (crosses). Colors

were obtained using B , R and K' 5 arcsec aperture magnitudes: aperture magnitudes avoid problems introduced by the different sampling of the galaxy profile in each band due to the different depth of the images. A 5 arcsec diameter aperture gives reliable colors being at least 3 times larger than the typical FWHM both in the IR and optical images. It is clearly visible that in the $(B - R)$ - $(R - K')$ plane stars and galaxies are not distinguishable, the two categories being heavily intermixed. Thus, in our case, a classification based on this method, which would be applicable only to 14 out of the 51 fields, would imply the rejection of a non-negligible fraction of galaxies (mainly blue galaxies) and a strong star contamination. However, we note that the use of the I , as in the case of Gardner et al. (1995b), instead of the R filter reduces such effect, even if cannot completely eliminate it (see Fig. 8 in Cowie et al. 1994).

The method of the K' isophotal area would have the advantage of being applicable to all our fields. In Fig. 4 K' isophotal area vs K' magnitude is plotted. The starred symbols are the objects independently classified as stars while circles are galaxies. Stars separate very well from galaxies down to $K' \sim 15$, but fainter than that, galaxies tend to mix up with point-like sources. Given the resolution of our IR images, this method would tend to discard the more compact galaxies.

We also compared the FOCAS classification obtained from the optical images with the one from the IR frames. In Fig. 5 the ratio between the number of objects classified as stars on the IR frames (S_K) and that on the B and R frames (S_{BR}) as a function of K' magnitude is shown: the IR based classification systematically underestimates the number of stars. As a result of this analysis, we decided to use two different and independent methods to correct the number counts for star contamination. The first method is based on the FOCAS classification performed on the IR images over the whole range of magnitudes and corrected in each magnitude bin for the underestimate shown in Fig. 5. At magnitudes fainter than $K' = 18$ we assumed the same correction obtained in the bin $17 < K' < 18$. The second method is based on the galaxy model of Cohen (1993) and has been used only for the fields of ESOKS2. In this case, since star counts are strictly dependent on galactic coordinates, we grouped our fields in three galactic latitude bins: low ($b > -40^\circ$), high ($-60^\circ < b < -40^\circ$) and pole ($b < -60^\circ$), and for each of them we estimated the expected number of stars down to $K' \sim 20$. It is worth noticing that the predicted star counts agree very well with the number of observed stars in the optical images. A more detailed discussion of the stellar contamination results obtained using this galaxy model is presented in Cohen and Saracco (1997).

6. Results

6.1. Galaxy Counts

The second selection criterion for our fields required the presence of 2 medium brightness stars to optimize the stacking of the frames. Although these objects were classified as stars in the ESO-SRC based COSMOS catalog, a fraction ($\sim 30\%$) turned out to be galaxies, both on the basis of the FOCAS classification and on a visual inspection of the frames. In order to prevent a bias toward bright galaxies, such galaxies have not been taken into account in deriving the galaxy number counts.

A small fraction of detections, 5% in the ESOKS1 (9 objects) and 7% in the ESOKS2 (71 objects), are sources lying near the edges of a frame, for which we cannot correctly estimate their magnitudes. We can either reject such detections reducing the useful area of the images (as in Driver et al. 1995), or assume for them a given magnitude and star fraction distribution. As in both cases some assumptions have to be made (the area to be discarded in the first case, and the source flux distribution in the second case), we have checked how much the overall results are affected by adopting one or the other of these approaches. We compared the results obtained adopting two different rejection areas (a strip 4 times and 2 times the minimum detection radius all around the images) or keeping all detections and assuming that their magnitude distribution and star fraction distribution reflect that obtained from all the other sources. The maximum discrepancy in the number density of sources was less than 4%. Thus, we have retained all detections in order to maximize the number of objects and the total surveyed area.

Then we corrected the object counts for spurious detections and incompleteness, using the results of the simulations. Finally, we subtracted the contribution from the stars according to the procedure described in §5.2.

The resulting galaxy counts for the ESOKS1 and ESOKS2 are listed in Table 4 and Table 5 respectively, where we report for each magnitude bin the effective area, the raw counts including stars (Raw), the counts corrected for edge sources, incompleteness and star contamination according to the properly scaled FOCAS classification (n), the counts N per square degree and the 1σ Poissonian error calculated as the square root of the raw counts. For the ESOKS2 (Table 5), we also report the counts obtained by subtracting the number of stars given by Cohen’s galaxy model (n_{mod} and N_{mod}), the raw number of sources (galaxies and stars, $\text{Raw}_{b < -75^\circ}$) and the number per magnitude bin per square degree ($C_{b < -75^\circ}$) detected in the 16 fields at galactic latitude $b < -75^\circ$. Since we expect that the contribution of stars at these latitudes is negligible at magnitudes fainter than $K' = 18$, these counts represent an upper limit to our galaxy counts and at the same time a

good landmark for our star counts.

In Fig. 6 the galaxy counts derived from the ESOKS1 and ESOKS2 are shown. The agreement between our two independent surveys is very good, the larger difference being within 1σ . The counts follow a $d\log N/dm$ relation with a slope of ~ 0.35 in the magnitude range $17 < K' < 20$, both in the ESOKS1 and in the ESOKS2. At brighter magnitudes ($K' < 17$) the counts slope is ~ 0.57 , as derived from the ESOKS2 data.

6.2. Field-to-Field Variations

Galaxy counts differ from field to field. The scatter on the number of galaxies detected in each field is $\sigma_{N_1} = 4.7$ for ESOKS1 (here we considered only the 7 fields with $t_{exp} = 54$ min, in order to have the same completeness limits) and $\sigma_{N_2} = 4.9$ for ESOKS2 (in this case we excluded low galactic latitude fields, because of the much higher star contamination). Given the mean number of galaxies per field ($\bar{N}_1 \sim 13$ and $\bar{N}_2 \sim 10$ for ESOKS1 and ESOKS2 respectively), we expect a pure poissonian noise of $\sigma_{p_1} = 3.6$ and $\sigma_{p_2} = 3.1$ galaxies per field. Another contribution to field to field variation is due to galaxy clustering. For an angular correlation function with a power-law form $w(\theta) = A_w\theta^{-\gamma}$ and a circular window function of radius θ_0 , the expected fluctuations due to clustering are:

$$\sigma_\omega = f(\gamma)w(\theta)^{1/2}\bar{N} \quad (2)$$

where $f(\gamma) \sim 1$. Brainerd et al. (1994) show that $\log A_w \sim -0.3r_{lim}$ where r_{lim} is the magnitude limit of the sample. Assuming $< r - K > \sim 3$ mag we rescaled the values of A_w estimated by Brainerd et al. and extrapolated their results to $r_{lim} \sim 22.5$. We found $A_w \sim 1.47$ (with θ in arcsec). Since the area of each field (~ 3.2 arcmin²) corresponds to a circle of radius $\theta_0 \sim 60''$ the expected field-to-field variation due to clustering is $\sigma_\omega \sim 3.1$ galaxies. Combining σ_ω with σ_p we expect $\sigma_{exp1} = 4.8$ and $\sigma_{exp2} = 4.4$ galaxies per field, both consistent with the measured values of σ_N .

6.3. Galaxy Colors

Visible-NIR colors and classifications of objects are available for the low galactic latitude fields. At $K' \sim 18$, the classification is reliable for 85% of the IR sources: 204 out of the 214 sources brighter than $K' = 18$ have been detected in B; 115 of them are stars, 66 are galaxies and the remaining 23 are unclassified sources. In Fig.7 we show the $B - K'$ vs K' diagram for the 66 galaxies (open circles) the unclassified $K' \leq 18$ sources (crosses) and the remaining $K' > 18$ objects (filled circles).

From Fig. 7 it is apparent that there is a small but non-negligible fraction of galaxies (9 galaxies) with $B - K' \leq 3$ at $K' \leq 18$. It is worth noticing that the IR photometric errors at these magnitudes are not larger than 0.1 mag and therefore the uncertainties in color estimation are also ~ 0.1 mag. These galaxies represent $\sim 10\%$ of our $K' \leq 18$ sample, and their very blue colors suggest the presence of star-formation activity. The three bluest galaxies, with a $B - K'$ colors of 1.8, 1.8 and 2.2 respectively, also show very blue B-R colors, 0.9, 0.7 and 0.8 respectively. The $B - K$ vs M_K relation (Saracco et al. 1996) suggests that galaxies brighter than $K' \sim 18$ and bluer than $B - K \sim 2.5$ should be at a redshift $z < 0.27$, whilst the expected median redshift of a sample limited to $K \sim 18$ is $z > 0.35$. In other words, this population of blue galaxies should be intrinsically fainter than L^* . We suggest that they could represent a population of blue sub- L^* galaxies similar to those evidenced by Lilly et al. (1995) at $z < 0.2$. The absence of this population from most of the other K -band selected samples is a natural consequence of the blank field selection criterion (e.g. Hawaii Deep Survey (HDS); ESOKS1; McLeod et al. 1995). Moreover a star-galaxy separation based on the color-color diagram may also introduce a bias against such blue galaxies.

In Fig. 8 the $B - K'$ color distribution for the $K' \leq 18$ ESOKS2 sample of galaxies (solid line) is compared to the HMDS sample (Gardner et al. 1995). 10 ESOKS2 objects brighter than $K' = 18$ have not been detected in the B images. Our B limiting magnitude is $B \sim 24$ and these objects are fainter than $K' \sim 17.5$. Thus the 10 undetected sources are redder than $B - K = 6$ and our color distribution is complete for $B - K' \leq 6$ (see also Fig. 7). These 10 sources are represented in Fig. 8 by the shaded boxes which represent the distribution of their $B - K'$ lower limits. The HMDS was derived by surveying the SSA blank selected fields and the Durham (Dur) fields, which are not 'blank'. Since also the two HMDS subsamples include lower limits to the $B - K$ color of some sources, we make use of a survival analysis technique (Avni et al. 1980; Isobe et al. 1986; Feigelson & Nelson 1985) to compare the colors of the ESOKS2 and the HMDS subsamples. The color distributions of the two HMDS subsamples shown in Fig. 8 are different at a very high confidence level: the probability that the two samples have been extracted from the same parent population is less than 10^{-4} as given by the generalized Wilcoxon test. We reach the same statistical conclusion by comparing the ESOKS2 sample with the HMDS-SSA sample, a result which could be not surprising given the different criteria used to select the HMDS-SSA fields and the ESOKS2 fields. On the contrary, the color distribution of the ESOKS2 sample is in good agreement with the HMDS-Dur sample as confirmed by the probability of 15% that the ESOKS2 and the HMDS-Dur samples are drawn from the same population.

7. Discussion

The sample we selected is fundamentally different from previous samples since it is composed by a high number of randomly selected and unconnected small fields, rather than by adjacent targets or unconnected large areas. We compare our results with each one of the samples present in the literature. We show that our counts are systematically lower at magnitudes fainter than $K' = 17$ even if the results are within the uncertainties due to count fluctuations for most of the samples.

Fig. 9 shows the counts derived by Gardner et al. (1996, Gar97), McLeod et al. (1995, McL95), Glazebrook et al. (1994, Gla94), Djorgovski et al. (1995, Djo95), Soifer et al. (1994, Soi94), Moustakas et al. (1997, Mou97) Gardner et al. (1993, HWS, HMWS, HMDS, HDS) and Mobasher et al. (1986 Mob86). The error bars represent \sqrt{N} statistics. We shall distinguish three different domains: $K < 16$, $16 < K < 20$ and $K > 20$.

At bright magnitudes ($K < 16$), the counts follow a linear $d\log N/dm$ relation with a slope very close to the Euclidean one ($d\log N/dm = 0.6$). In this magnitude range the counts of Gardner et al. (1996), Glazebrook et al. (1994) and Mobasher et al. (1986) agree very well, while a larger scatter is introduced by the HWS and HMWS ones (Gardner et al. 1993; Gardner 1995a).

In the intermediate magnitude range ($16 < K < 20$) a bump with respect to both the brighter and the fainter magnitude ranges is visible. Such a feature is not present in the B , R and I -band galaxy counts at comparable magnitudes (e.g. Tyson 1988; Metcalfe et al. 1991; Metcalfe et al. 1995, Driver et al. 1995). Gardner et al. (1993) interpret this feature as a flattening of the count slope to 0.26 at $K > 17$, which implies a remarkable blueing trend of galaxies at these magnitudes (Cowie et al. 1995). On the other hand, in the same magnitude range, the galaxy counts of McLeod et al. (1995) suggest a steeper slope (0.32) and the deep counts of Soifer et al. (1994), although systematically higher than the others, confirm such steeper slope.

At faint magnitudes ($K > 20$) the $d\log N/dm$ is not very well defined, as shown by the quite different shape and surface density derived from the HDS and the Djorgovski et al. (1995) data: while the HDS counts linearly rise up to $K \sim 19.5$ and then clearly decline, the Djorgovski et al. counts continue to rise with a power-law slope of 0.32 with no evidence of a turnover or of a flattening down to the limits of the survey ($K \sim 24$).

Fig. 10 shows ESOKS1 and ESOKS2 galaxy counts superimposed to those in the literature. At magnitudes brighter than $K' \sim 16.5$ our counts perfectly agree with those of Glazebrook et al. (1994), Gardner et al. (1996), Mobasher et al. (1986) and the HMWS; note that in this magnitude range our surveys cover a much smaller area than the other

authors’. At fainter magnitudes, where we surveyed a larger area than other authors did, our counts are systematically lower than those of HMDS and HDS, McLeod et al. (1995) and Soifer et al. (1994) and do not show the bump found by these surveys at these magnitudes.

Many factors may contribute to justify differences between counts derived from different surveys: field selection criteria, magnitude estimate, correction for star contamination, width and sampling of the surveyed areas. The bias produced by a blank field selection criterion, often adopted in faint galaxy count surveys, significantly affects counts only at $K < 16$, and it is negligible at fainter magnitudes (§2.1). In principle, different methods of estimating magnitudes could make a comparison more difficult. On the other hand, magnitudes can all be reconducted to a “total” magnitude (e.g. by using standard growth curves), even if some uncertainties are necessarily introduced. On the contrary, the correction for star contamination (e.g., through color-color diagrams) depends on the filters used and different results could be affected by different effects. And, last but not least, different area widths are affected by count fluctuations and, for a given surveyed area, fluctuations may depend on the number of fields which sample the area and on their distribution on the sky (sparse or adjacent fields).

The number counts of Soifer et al. (1994), obtained over an area of ~ 2.4 arcmin², appear to be significantly higher than the others, in particular the difference between our and their surface density of galaxies in the magnitude range $16 < K' < 19$ is ~ 12000 galaxies per square degree (~ 8 galaxies on 2.4 arcmin²). Soifer et al.’s counts were obtained surveying areas surrounding high-redshift target objects and they are not corrected for star contamination. Magnitudes are estimated within 3'' and corrected to total magnitude by summing the mean value of the difference between the 3'' and a larger aperture magnitude for a sample of bright objects. We tried to reproduce this method by estimating the $K'_{3''_{corr}}$ magnitude for the sources of the ESOKS2, summing the median value of the difference $K'_{5''} - K'_{3''}$ to the 3'' aperture magnitude. In Fig. 11 the number counts obtained using the $K'_{3''_{corr}}$ magnitude are compared to those obtained with FOCAS K'_{tot} magnitude. The agreement between the two distributions is quite good, thus showing that the large discrepancy between our counts and those derived by Soifer et al. (1994) cannot be ascribed to different magnitude estimates. In an attempt to establish if the observed count fluctuations can be responsible of such excess obtained over an area of 2.4 arcmin², from the 38 ESOKS2 high galactic latitude fields we randomly extracted a number of fields corresponding to such area (one field in this case). By repeating N times the procedure and computing the surface density of galaxies each time, we estimate that the probability to obtain the same number counts of Soifer et al. (1994) over an area of 2.4 arcmin² is 4%. This low probability is marginally significant, but taking into account the star contamination

which affects the Soifer et al.’s sample, the surface density is probably compatible with count fluctuations. We feel however that, in this magnitude range, such high surface density may reflect a real high density region, maybe related to the peculiar selection criterion adopted for the target areas and the missing correction for star contamination.

McLeod et al. (1995) used FOCAS total magnitudes, as we did. They surveyed an area of ~ 22 arcmin² divided in two separate fields. Star-galaxy separation has been done on the basis of a color-color diagram. They count an excess of 5600 galaxies per square degree (34 galaxies on 22 arcmin²) with respect to our data in the magnitude range $16 < K' < 19$. We estimated that the probability to observe the surface density found by McLeod et al. (1995) over ~ 22 arcmin², corresponding to ~ 7 ESOKS fields, is 3%, which implies that the observed count fluctuations alone cannot justify the discrepancy between our and their counts.

In the case of HMDS (Gardner 1995a), which shows the highest surface density of galaxies down to $K \sim 18$, the excess with respect to our data is ~ 6600 gal/deg² in the magnitude range $16 < K' < 19$. Taking into account that we surveyed approximately the same area down to $K' = 18$ (~ 170 vs ~ 160 arcmin²), such discrepancy cannot be explained in terms of count fluctuations only. In the HMDS sample, the magnitudes are calculated within an aperture of $6''$ which is not significantly different from an aperture of $5''$. In Fig. 2 we did show that the $K'_{5''}$ and K'_{tot} magnitude distributions do not differ, as confirmed also by a KS-test, thus implying that the different counts are not due to the different magnitudes used. Thus, in this case the difference cannot be reconduced to any of the above mentioned factors.

The discrepancy between the ESOKS2 and the HDS is smaller than with other surveys, the deviations being of the order of 1σ in each magnitude bin. The discrepancy is larger when compared to the ESOKS1 sample. The area covered by the HDS is ~ 16.5 arcmin² and their star-galaxy separation is based on the inverse second moment of the light distribution (Kron 1980) and the color-color diagram. Magnitudes are estimated within $3''$ and corrected to total magnitude by summing the median value of the difference computed between $6''$ and $3''$ aperture magnitudes for a sample of isolated objects (Cowie et al. 1994). We have already shown how the different magnitudes used cannot explain the observed discrepancies (see Fig. 10). The HDS surface density of galaxies in the magnitude range $16 < K < 19$ is a factor ~ 1.35 larger than that derived from the ESOKS2 (corresponding to an excess of 3900 galaxies per square degree) and a factor 1.7 larger than that obtained from the ESOKS1. In terms of pure count fluctuations, the probability to observe such surface density over ~ 16.5 arcmin² is 10%. Thus the discrepancy between our counts and those derived by the HDS is consistent with count fluctuations.

8. Summary and Conclusions

We have presented galaxy counts in the magnitude range $13 < K' < 20$, derived from two independent surveys covering ~ 40 arcmin² (ESOKS1) and ~ 170 arcmin² (ESOKS2) in the Southern Hemisphere. Our counts are in quite good agreement with those of other authors at bright magnitudes ($K' < 16 - 17$), and follow a $d\log N/dm$ relation with a slope of 0.57. At fainter magnitudes ($K' > 17$), our counts are systematically lower than the others and do not show the bump seen in other K -band surveys. Such a discrepancy cannot be accounted for in terms of the different magnitudes used while could be consistent with count fluctuations in most cases. On the other hand the systematic nature of the discrepancy makes significant the absence of the bump in our data at magnitudes $K' > 17$. It is more difficult to quantify the uncertainty in our counts due to the methods we were forced to use in order to subtract the star contribution, even if at $K' > 17$ the expected number of stars is relatively low. A clue is given by the source counts (i.e. galaxies and stars) which we obtained on the 16 high galactic latitude fields (see Table 5): these counts are necessarily upper limits to the galaxy counts and they unambiguously confirm the discrepancy with other authors and exclude its dependency from the uncertainties in our star correction methods.

Our counts support the conclusions of Gardner et al. (1993) of a changing in the slope of the $d\log N/dm$ relation at $K' \sim 17$, confirming the blueing trend of faint galaxies shown by Cowie et al. (1995). However, we measure a $d\log N/dm$ slope (0.35 at $K' \geq 17$) in agreement with those found by McLeod et al. (1995) and Djorgovski et al. (1995) but higher than the value of 0.26 found by Gardner et al. (1993).

In the ESOKS2 subsample limited to $K' \sim 18$, we detect a significant fraction (10%) of very blue galaxies ($B - K' < 3$). This population is not present in other K -band selected samples. Such deficiency is expected in surveys where a blank-field selection criterion has been applied (e.g. HMDS; HDS; ESOKS1; McLeod et al. 1995). The very blue $B - K'$ and $B - R$ colors of such a population indicates that they are star-forming galaxies. From the $B - K$ vs M_K relation (Saracco et al. 1996) we infer that they have low luminosities and are at redshifts $z < 0.27$. They may represent a population of blue sub- L^* galaxies similar to that previously suggested by Lilly et al. (1995) at $z < 0.2$.

We are grateful to A. Moorwood and C. Lidman for advice on the use of IRAC2 and to L. L. Cowie for suggestions on the data analysis procedures. Special thanks are due to M. Cohen, who provided us with the output of his SKY galaxy model suited to our fields.

REFERENCES

- Abraham R. G., Tanvir N. R., Santiago B. X., Ellis R. S., Glazebrook K. & van den Bergh S. 1996, MNRAS, 279, L47
- Avni Y., Soltan A., Tanambaum H. & Zamorani G. 1980, ApJ, 235, 694
- Banchet V., Mamon G. A. & Contensou M 1997, Astr. Lett. & Comm., in press
- Bernstein G. M., Nichol R. G., Tyson J. A., Ulmer M. P. & Wittman D. 1995, AJ, 110, 1507
- Bershady M. A. et al. 1994, AJ, 108, 870
- Bertin E. & Dennefeld M. 1997, A&A, 317, 42
- Brainerd T. G., Smail I. R. & Mould J. R. 1994, BAAS 185, 114.06
- Broadhurst T. J., Ellis R. S. and Glazebrook K. 1992, Nat. 355, 55
- Cohen M. 1993, AJ 105, 1860
- Cohen M. & Saracco P. 1997, in preparation
- Colless M. M., Ellis R. S., Broadhurst T. J., Taylor K. & Peterson B. A. 1993, MNRAS, 261, 19
- Colless M. M., Schade D., Broadhurst T. J. & Ellis R. S. 1994, MNRAS, 267, 1108
- Cowie L. L., Gardner J. P., Lilly S. J. & McLean I. 1990, ApJ, 360, L1
- Cowie L. L., Songaila A. and Hu E. M. 1991, Nat. 354, 460
- Cowie L. L., Gardner J. P., Hu E. M., Songaila A., Hodapp K. W. & Wainscoat R. J. 1994, ApJ, 434, 114
- Cowie L. L., Hu E. M. & Songaila A. 1995, AJ, 110, 1576
- Djorgovski et al. 1995, ApJ, 438, L13
- Driver S. P., Windhorst R. A. & Griffiths R. E. 1995, ApJ, 453, 48
- Driver S. P., Couch W. J., Phillipps S. & Windhorst R. A. 1996, ApJ, 466, L5
- Elias J. H., Frogel J. A., Matthews K. & Neugebauer G. 1982, AJ, 87, 1029

- Feigelson E. D. & Nelson P. I. 1985, *ApJ*, 293, 192
- Gardner J. P., Cowie L. L. & Wainscoat R. J. 1993, *ApJ*, 415, L9
- Gardner J. P. 1995a, *ApJS*98, 441
- Gardner J. P. 1995b, *AJ*, 452, 538
- Gardner J. P., Sharples R. M., Carrasco B. E. & Frenk C. S. 1996, *MNRAS*, 282, L1
- Glazebrook K., Peacock J., Collins C. & Miller L. 1994, *MNRAS*, 266, 65
- Glazebrook K., Ellis R., Santiago B. & Griffiths R. 1995, *MNRAS*, 275, L19
- Griffiths R. E. et al. 1994a, *ApJ*, 437, 67
- Griffiths R. E. et al. 1994b, *ApJ*, 435, L19
- Guiderdoni B. 1991, in *Annales de Physique*, 16, 235
- Hodapp K. W., Rayner J. & Irwin E. 1992, *PASP* 104, 441
- Huang J. S., Cowie L. L., Gardner J. P., Hu E. M., Songaila A., & Wainscoat R. J. 1997, *ApJ*, 476, 12
- Isobe T., Feigelson E. D. & Nelson P. I. 1986, *ApJ*, 306, 490
- Jarvis J. F. & Tyson J. A. 1981, *AJ*, 86, 476
- Jones L. R., Fong R., Shanks T., Ellis R. S. & Peterson B. A. 1991, *MNRAS*, 249, 481
- Kron R. G. 1980, *ApJS*43, 305
- Legget S. K. & Hawkins M. R. S. 1988, *MNRAS*, 234, 1065
- Lidman C., Gredel R. & Moneti A. 1995, *ESO Report n.2*, Aug. 1995
- Lilly S. J., Tresse L., Hammer F., Crampton D. & Le Fevre O. 1995, *ApJ*, 455, 108
- Maddox S. J., Sutherland W. J., Efstathiou G., Loveday J. & Peterson B. A. 1990, *MNRAS*, 247, 1
- Mamon G. A. 1995, in *Wide-Field Spectroscopy and the Distant Universe*, ed. S. J. Maddox & Aragon-Salamanca (Singapore: World Scientific)

- McLeod B. A., Bernstein G. M., Reike M. J., Tollestrup E. V. & Fazio G. G. 1995, *ApJS*96, 117
- Metcalfe N., Shanks T., Fong R. & Jones L. R. 1991, *MNRAS*, 249, 498
- Metcalfe N., Shanks T., Fong R. & Roche N. 1995, *MNRAS*, 273, 257
- Mobasher B., Ellis R. & Sharpless R. 1986, *MNRAS*, 223, 11
- Morwood A. et al. 1992, *Messenger* 69, 61
- Moustakas L. A., Davis M., Graham J. R., Silk J., Peterson B. A. & Yoshii Y. 1997, *ApJ*, 475, 44
- Saracco P., Chincarini G. & Iovino A. 1996, *MNRAS*, 283, 865
- Soifer B. T. et al. 1994, *ApJ*, 420, L1
- Tyson J. A. 1988, *A.J.* 96, 1
- Tyson J. A. 1989, in *CCDs in Astronomy*, ed. G. H. Jacoby, A.S.P. Conference Series 8, 1
- Valdes F. 1982, in *Faint Object Classification and Analysis System* (Tucson: NOAO)
- Wainscoat R. J. & Cowie L. L. 1991, *AJ*, 103, 332
- White S. D. M. 1989, in *The Epoch of Galaxy Formation*, ed. C. S. Frenk, R. S. Ellis, T. Shanks, A. F. Heavens & J. A. Peacock (Dordrecht: Kluwer), 15

Fig. 1.— Total FOCAS magnitude distribution (K'_{tot}) for the ESOKS1 sample

Fig. 2.— Distribution of total and aperture magnitudes of the ESOKS2 sample.

Fig. 3.— $B - R$ vs. $R - K'$ color-color plot for the optically classified objects (stars represent stars and open circles galaxies) and for the unclassified objects (crosses).

Fig. 4.— K' isophotal detection area vs. K'_{tot} magnitude. The symbols are as in Fig. 3.

Fig. 5.— Complement to 1 of the ratio between the number of objects which FOCAS classifies as stars on the IR frames (S_K) and on the B and R frames (S_{BR}) as a function of K' magnitude.

Fig. 6.— K' -band galaxy number counts derived from the ESOKS1 (starred symbols) and ESOKS2 (filled circle).

Fig. 7.— Color-magnitude diagram for the $K' \leq 18$ galaxies (open circles), the $K' \leq 18$ unclassified sources (crosses), and the $K' > 18$ unclassified objects (filled circles). Given that the B limiting magnitude differs from field to field, the two continuous lines represent the minimum and the maximum value of B_{lim} .

Fig. 8.— $B - K$ color distribution of the $K \leq 18$ ESOKS2 sample (solid thick line), the HMDS-SSA (dashed line), and the HMDS-Dur (dotted line) samples. The distributions are normalized to the same number of sources. The dashed histogram includes the lower limits to the $B - K$ color of the 10 ESOKS2 optically undetected sources.

Fig. 9.— K -band galaxy number counts from the literature. The continuous line shows a slope $d \log N / dm = 0.6$.

Fig. 10.— ESOKS1 and ESOKS2 galaxy number counts superimposed to those from the literature.

Fig. 11.— Galaxy number counts obtained by using total FOCAS magnitude are compared to those obtained by using $K'_{3''_{corr}}$ magnitudes.

Table 1: ESOKS1: list of observed fields

| <i>ID</i> | RA 2000 | Dec 2000 | <i>b</i> | <i>t_{exp}</i> min |
|-----------|------------|-------------|----------|-------------------------------|
| 0224-300 | 02 24 03 | -30 14 15 | -69 | 162 |
| 2351-250 | 23 51 52 | -25 07 53 | -77 | 162 |
| 0345-171 | 03 45 38 | -17 19 37 | -48 | 72 |
| 2239-275a | 22 40 03 | -27 57 38 | -62 | 72 |
| 2239-275b | 22 40 00 | -27 56 57 | -62 | 54 |
| 0044-222 | 00 44 32 | -22 25 15 | -85 | 54 |
| 0335-170 | 03 36 00 | -17 05 05 | -50 | 54 |
| 0337-105 | 03 37 03 | -10 55 54 | -47 | 54 |
| 0348-153 | 03 48 40 | -15 36 32 | -47 | 54 |
| 2240-295 | 22 40 25 | -30 09 58 | -62 | 54 |
| 2243-301 | 22 43 40 | -30 09 57 | -62 | 54 |
| 2359-265 | 23 59 57 | -26 56 27 | -79 | 36 |

Table 2: ESOKS2: list of observed fields

| <i>ID</i> | RA 2000 | Dec 2000 | <i>b</i> | <i>t_{exp}</i> min | B | R |
|-----------|------------|-------------|----------|-------------------------------|---|---|
| 1927-3904 | 19 27 54 | -39 04 58 | -24 | 36 | * | * |
| 1930-3743 | 19 30 54 | -37 43 06 | -24 | 36 | * | * |
| *tt1930 | 19 30 00 | -37 00 00 | -24 | 18 | | |
| 1930-3808 | 19 30 07 | -38 08 47 | -24 | 36 | * | * |
| 1931-4114 | 19 31 11 | -41 14 02 | -25 | 36 | * | * |
| 1935-3933 | 19 35 59 | -39 33 45 | -26 | 36 | * | * |
| 1941-4118 | 19 41 44 | -41 18 36 | -27 | 36 | * | * |
| 1943-3905 | 19 43 39 | -39 05 31 | -27 | 36 | * | * |
| 2110-3740 | 21 10 12 | -37 40 38 | -43 | 36 | * | * |
| 2113-4127 | 21 13 06 | -41 27 43 | -44 | 36 | * | * |
| 2113-3911 | 21 13 45 | -39 11 06 | -44 | 36 | * | * |
| 2114-3814 | 21 14 19 | -38 14 36 | -44 | 36 | * | * |
| 2115-3918 | 21 15 04 | -39 18 58 | -44 | 36 | * | * |
| 2123-3754 | 21 23 42 | -37 54 37 | -46 | 36 | * | * |
| 2127-4037 | 21 27 53 | -40 37 48 | -47 | 36 | * | * |
| 2227-2919 | 22 27 04 | -29 19 46 | -59 | 36 | | |
| 2233-2831 | 22 33 24 | -28 31 01 | -60 | 36 | | |
| 2234-2834 | 22 34 53 | -28 34 02 | -60 | 36 | | |
| 2236-3209 | 22 36 02 | -32 09 55 | -61 | 36 | | |
| 2237-3116 | 22 37 26 | -31 16 46 | -61 | 36 | | |
| 2240-2953 | 22 40 14 | -29 53 25 | -62 | 36 | | |
| 2241-2835 | 22 41 10 | -28 35 25 | -62 | 36 | | |
| 2246-2949 | 22 46 06 | -29 49 35 | -63 | 36 | | |
| 2353-3035 | 23 53 02 | -30 35 01 | -77 | 36 | | |
| 2354-2822 | 23 54 18 | -28 22 42 | -78 | 36 | | |
| 2354-2736 | 23 54 56 | -27 36 05 | -78 | 36 | | |
| 2356-2730 | 23 56 15 | -27 30 27 | -78 | 36 | | |
| 2357-3151 | 23 57 08 | -31 51 40 | -78 | 36 | | |
| 0006-2737 | 00 06 26 | -27 37 19 | -81 | 36 | | |
| 0010-3125 | 00 10 49 | -31 25 36 | -81 | 36 | | |
| 0035-3048 | 00 35 40 | -30 48 40 | -86 | 36 | | |
| 0038-3003 | 00 38 05 | -30 03 48 | -86 | 36 | | |
| 0042-3106 | 00 42 15 | -31 06 08 | -86 | 36 | | |
| 0049-3106 | 00 49 46 | -31 06 10 | -86 | 36 | | |
| 0056-3131 | 00 56 59 | -31 31 58 | -86 | 36 | | |
| 0101-2935 | 01 01 59 | -29 35 23 | -86 | 36 | | |
| 0110-2957 | 01 10 05 | -29 57 40 | -85 | 36 | | |
| 0114-3053 | 01 14 24 | -30 53 30 | -83 | 36 | | |
| 0116-3136 | 01 16 40 | -31 36 49 | -83 | 36 | | |
| 0212-2937 | 02 12 60 | -29 37 31 | -71 | 36 | | |
| 0215-3036 | 02 15 26 | -30 36 13 | -71 | 36 | | |
| 0217-3015 | 02 17 52 | -30 15 14 | -70 | 36 | | |
| 0221-3119 | 02 21 18 | -31 19 14 | -70 | 36 | | |
| 0227-3034 | 02 27 41 | -30 34 34 | -68 | 36 | | |
| 0333-1400 | 03 33 53 | -14 00 46 | -49 | 36 | | |
| 0337-1659 | 03 37 17 | -16 59 02 | -50 | 36 | | |
| 0338-1440 | 03 38 45 | -14 40 56 | -49 | 36 | | |
| 0340-1635 | 03 40 58 | -16 35 44 | -49 | 36 | | |
| 0341-1642 | 03 41 21 | -16 42 03 | -49 | 36 | | |
| 0342-1646 | 03 42 19 | -16 46 46 | -49 | 36 | | |
| 0347-1659 | 03 47 53 | -16 59 50 | -48 | 36 | | |

Table 3: Completeness corrections as a function of exposure time

| K' | c | | | | |
|-----------|-------|-------|-------|-------|-------|
| t_{exp} | 162 | 72 | 54 | 36 | 18 |
| 18.0-18.5 | 1.000 | 1.000 | 1.000 | 1.000 | 1.042 |
| 18.5-19.0 | 1.000 | 1.000 | 1.020 | 1.083 | 1.720 |
| 19.0-19.5 | 1.000 | 1.070 | 1.300 | 2.222 | ... |
| 19.5-20.0 | 1.045 | 1.640 | 3.220 | ... | ... |

Table 4: K' -band number counts: ESOKS1

| K' | Area arcmin ² | Raw | n | N | σ_N |
|-------|-----------------------------|-----|-------|-------|------------|
| 16-17 | 39.2 | 23 | 11.5 | 1056 | 440 |
| 17-18 | " | 28 | 24.2 | 2222 | 485 |
| 18-19 | " | 62 | 59.0 | 5418 | 723 |
| 19-20 | 35.9 | 68 | 113.0 | 11326 | 864 |

Table 5: K' -band number counts: ESOKS2

| K' | Area arcmin ² | Raw | n | n_{mod} | N | N_{mod} | σ_N | Area _{$b < -75^\circ$} arcmin ² | Raw _{$b < -75^\circ$} | $C_{b < -75^\circ}$ |
|-------|-----------------------------|-----|-------|-----------|------|-----------|------------|--|--|---------------------|
| 13-14 | 166.9 | 9 | 2.2 | 0.8 | 47 | 18 | 64 | 52.2 | 2 | 138 |
| 14-15 | " | 24 | 3.9 | 4.0 | 85 | 87 | 106 | " | 3 | 207 |
| 15-16 | " | 57 | 16.7 | 22.8 | 363 | 494 | 163 | " | 11 | 758 |
| 16-17 | " | 117 | 56.0 | 59.0 | 1205 | 1278 | 235 | " | 21 | 1447 |
| 17-18 | " | 221 | 138.0 | 120.0 | 2994 | 2596 | 322 | " | 52 | 3582 |
| 18-19 | " | 423 | 312.0 | 291.0 | 6756 | 6303 | 446 | " | 95 | 6876 |